Correspondence to:
J. M. Torta,
jmtorta@obsebre.es

Improving the modeling of geomagnetically induced currents in Spain

J. M. Torta[1] [iD], **A. Marcuello[2]** [iD], **J. Campanyà[3]** [iD], **S. Marsal[1]** [iD], **P. Queralt[2]** [iD], and **J. Ledo[2]**

[1]Observatori de l'Ebre, (OE), CSIC - Universitat Ramon Llull, Roquetes, Spain, [2]Institut Geomodels, Departament de Dinàmica de la Terra i de l'Oceà, Universitat de Barcelona, Barcelona, Spain, [3]School of Physics, Trinity College Dublin, Dublin, Ireland

Abstract Vulnerability assessments of the risk posed by geomagnetically induced currents (GICs) to power transmission grids benefit from accurate knowledge of the geomagnetic field variations at each node of the grid, the Earth's geoelectrical structures beneath them, and the topology and relative resistances of the grid elements in the precise instant of a storm. The results of previous analyses on the threat posed by GICs to the Spanish 400 kV grid are improved in this study by resorting to different strategies to progress in the three aspects identified above. First, although at midlatitude regions the source fields are rather uniform, we have investigated the effect of their spatial changes by interpolating the field from the records of several close observatories with different techniques. Second, we have performed a magnetotelluric (MT) sounding in the vicinity of one of the transformers where GICs are measured to determine the geoelectrical structure of the Earth, and we have identified the importance of estimating the MT impedance tensor when predicting GIC, especially where the effect of lateral heterogeneities is important. Finally, a sensitivity analysis to network changes has allowed us to assess the reliability of both the information about the network topology and resistances, and the assumptions made when all the details or the network status are not available. In our case, the most essential issue to improve the coincidence between model predictions and actual observations came from the use of realistic geoelectric information involving local MT measurements.

1. Introduction

A time-varying magnetic field induces an electric field according to Faraday's induction law. On the occasion of severe geomagnetic storms, this electric field acts as a voltage source for the high-voltage power transmission grids, so that the related currents, known as geomagnetically induced currents (GICs), may disrupt or damage the transformers of those grids. This is perhaps the space weather threat of most concern in our era. A symptom of this fact is that scientific journals dedicate special issues to this topic [e.g., *Knipp*, 2015; *Pulkkinen*, 2016], and an increased awareness and interest of decision makers and government leaders is certainly detected [*Jonas and McCarron*, 2015; *Baker*, 2016].

Although one generally expects that at middle to low latitudes the magnitude of GICs is 1 order of magnitude lower than that at high latitudes [*Pulkkinen et al.*, 2012], recently there has been a great wealth of studies on the vulnerability assessment at those middle to low latitude grids [e.g., *Demiray et al.*, 2013; *Liu et al.*, 2014; *Torta et al.*, 2014; *Barbosa et al.*, 2015; *Zhang et al.*, 2015; *Blake et al.*, 2016]. The increasing concern about GICs as an emergent natural hazard has been boosted by the evidence that power system disturbances can be associated with the occurrence of geomagnetic sudden commencements (SCs) at those lower latitudes [*Kappenman*, 2003; *Torta et al.*, 2014; *Fiori et al.*, 2014; *Carter et al.*, 2015].

To be efficient, such vulnerability analyses must benefit from the following.

1. *The knowledge of the geomagnetic field variations at each node of the grid*. The degree of their homogeneity depends on the geomagnetic latitude, and resorting to the spherical elementary current systems (SECS) [*Amm and Viljanen*, 1999] has revealed to be an effective method of interpolation from a network of geomagnetic stations providing measurements [*McLay and Beggan*, 2010].
2. *The knowledge of the Earth's geoelectrical structures beneath the network*. Abrupt site-to-site differences in the derived geoelectric field because of the ocean-land interfaces [e.g., *Piña-Varas et al.*, 2014, 2015; *Pirjola*, 2013; *Gilbert*, 2014] or the juxtaposition of provinces with old and cold rocks that are largely devoid of electrical conducting mineral phases with deep intracontinental basins filled with conductive sedimentary rocks can show geographically distributed differences up to a factor of 1000 [e.g., *Campanyà et al.*, 2011, 2012; *Bedrosian and Love*, 2015; *Ledo et al.*, 2011; *Rosell et al.*, 2011].
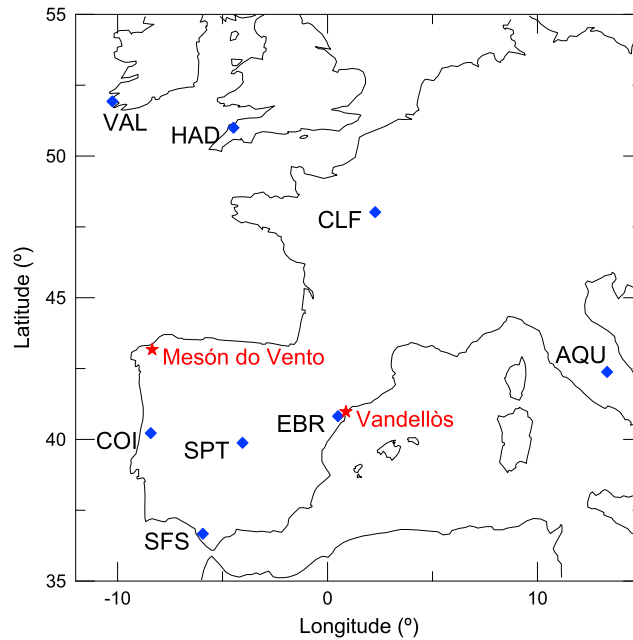
Figure 1. Location of the substations (red symbols) and the geomagnetic observatories (blue symbols, identified by their three-letter IAGA code) used in this study.

3. *The knowledge of the topology and the relative resistances of the power grid elements in the precise instant of the geomagnetic storm* [*Torta et al.*, 2014].

The combination of all the above mentioned factors in a worst case scenario can make the storm time geoelectric induction reach hazardous levels at a local scale. Regarding the hazard assessment, upper limits for the potentially biggest geomagnetic storm or estimates of return periods of a hypothetical extreme event are thus of great value, which causes studies on probability of extreme values to proliferate [e.g., *Thomson et al.*, 2011; *Pulkkinen et al.*, 2012; *Love*, 2012; *Ngwira et al.*, 2015; *Nikitina et al.*, 2016; *Wintoft et al.*, 2016; *Riley and Love*, 2017].

Previous works of *Torta et al.* [2012, 2014] analyzed the threat posed by GICs to the Spanish 400 kV power transmission grid. In spite of their satisfactory results, these studies revealed that there was substantial scope for improvement in the three points listed before. This paper sets out our findings in the attempt of improving our previous results in these three points with regard to modeling GICs in the Spanish power network, namely, the availability of geomagnetic data, the Earth's geoelectrical response, and the power network status.

2. Experimental Design

2.1. Interpolation of Geomagnetic Field Variations

GIC computation at a given substation of the grid can be carried out by the use of data from the nearest geomagnetic observatory. However, there are areas of the Spanish power transmission grid that are far from any observatory (Figure 1). In order to obtain a good representation of the geomagnetic variations (and thus the geoelectric field) at these sites, we have explored different techniques of field continuation from the records of a set of ground-based observatories.

Nearest neighbor (NN). For each horizontal component of the magnetic field separately, this method simply consists in using the magnetic variations of the nearest observatory at a given location.

Linear interpolation using Delaunay triangulation (LD). For each horizontal component of the magnetic field separately, this technique determines the unique planar surface passing through the ordinates at each triangle of observatory sites obtained by Delaunay triangulation [*Delaunay*, 1934].

Magnetic scalar potential (V). A 2-D polynomial is adjusted to the magnetic scalar potential V, so that $-\overrightarrow{\nabla}_h V = \overrightarrow{B}_h$, where $\overrightarrow{B}$ is the magnetic field, and the subscript h denotes the horizontal projection of the vector field [e.g., *Düzgit et al.*, 1997]. Different degrees have been tested for the polynomials, ranging from 1 to 5.

Spherical elementary current systems (SECS). This method, introduced by *Amm* [1997] and developed by *Amm and Viljanen* [1999], consists in computing the equivalent current system flowing at constant height sources (at least the ionospheric E layer but also at a certain depth below the Earth's surface) yielding the set of magnetic variations observed at the ground magnetometer sites. We have explored both external only (110 km height) and combined external/internal (-100 km) sources.
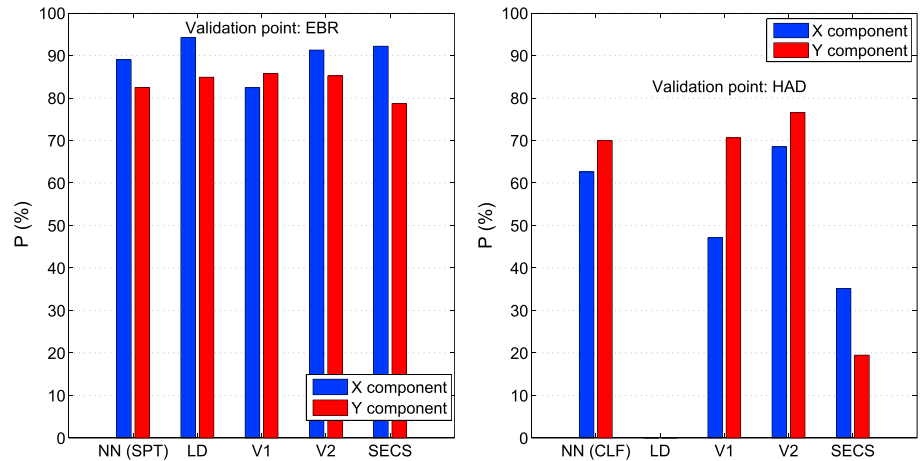
Figure 2. Comparison between different field continuation methods (see main text) evaluated in terms of the performance parameter, P, for the Halloween event (29–31 October 2003). Note that P is expressed as a percentage, i.e., hundredfold the value of equation (1). The figures correspond to (left) EBR and (right) HAD as validation observatories; blue and red bars correspond to the X (north) and Y (east) components of the magnetic field, respectively. Note that the LD method is not available for HAD, by reason of the fact that it is peripheral in our network. The presented SECS method uses external sources only, a rectangular grid with latitude boundaries (24°, 69°), longitude boundaries (−11°, 16°), and a grid spacing of 1.5°× 1.5°.

The first two methods are purely mathematical, while the other two are physically based. Our network comprises different midlatitude observatories of western Europe (see Figure 1), in particular, SFS (−5.9°E, 36.7°N geodetic), SPT (−4.3°E, 39.5°N), COI (−8.4°E, 40.2°N), EBR (0.5°E, 40.8°N), AQU (13.3°E, 42.4°N), CLF (2.3°E, 48.0°N), and HAD (−4.5°E, 51.0°N). Each interpolation method above is evaluated by comparing observed versus modeled magnetic field variations at a given validation observatory, after ignoring the data corresponding to that validation point in the model input. The quantitative comparison was initially made based on the linear correlation coefficient (ρ), but since modeled observations with the same signal multiplied by a scale factor or shifted by a constant value will provide the same ρ, we prefer to base the comparison on the residuals of both time series, according to the performance parameter (P) [e.g., *Torta et al.*, 2014; *Marsal et al.*, 2017] defined as

$$P = 1 - \frac{1}{\sigma_0}\sqrt{\frac{\sum_{i=1}^{N}\left[(o_i - \overline{o}) - (m_i - \overline{m})\right]^2}{N}}, \tag{1}$$

where o_i and m_i are the ith (out of a total of N) observed and modeled values, respectively (i.e., those at time t_i), $\overline{o}$ and $\overline{m}$ are their respective means, and σ_0 is the standard deviation of the observations. Note that unlike *Torta et al.* [2014], and because we are rather interested in temporal variations, here we have subtracted the corresponding mean values from both the observed and modeled data sets. This in turn avoids misfits coming from measuring offsets of thermal origin, magnetic anomalies, or others. P values close to unity (or to 100 if we use a percent scale) reflect a good behavior of modeling.

Our analysis was carried out for two remarkable space weather events: Halloween storm (29–31 October 2003) and the 2015 St. Patrick's Day storm (17–18 March 2015). Figure 2 corresponds to the first event, and it displays a comparative bar plot of P versus the interpolation method. Figure 2 (left) shows the results for EBR as the validation point, which is the closest to the centroid of the distribution, while Figure 2 (right) corresponds to HAD, the northernmost site. In general, the same gross features are obtained for the other event analyzed (not shown here). The first noticeable aspect is that the different methods perform considerably well for the lower latitude observatories of the network, exemplified in the figure by EBR. The results are not so good for HAD, mainly because it is located at the periphery of the network. Regarding the adequateness of the interpolation techniques, no remarkable differences are appreciated at EBR, where the simplest method, NN, yields results that are comparable to the others. Obviously, the effectiveness of this latter method highly depends on the distance to the nearest observatory, which is rather close in
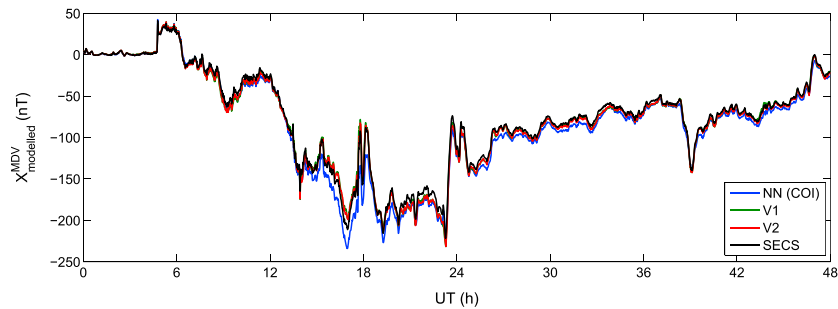
Figure 3. Modeled *X* component of the magnetic field at Mesón do Vento substation during the St. Patrick's storm event (17–18 March 2015) using different extrapolation techniques: NN (blue line), V1 (green), V2 (red), and SECS (black). Note that LD method is not available at this peripheral point.

this case. Surprisingly, the purely mathematical LD method gives the best results at EBR for the *X* component. As for HAD, the best results are obtained with the V2 method (polynomial of degree 2 for the magnetic scalar potential).

Despite that SECS have been shown to give good results at high latitudes, our tests confirm, as concluded by *McLay and Beggan* [2010], that this technique is not always the most suitable one at middle latitudes for interpolation purposes. As already noted by *Amm and Viljanen* [1999], we have observed that the design of the grid where the poles of the elementary currents are located is not a minor point. In particular, the density of poles and the location of the boundaries of the grid area have a notable influence on the SECS method performance. Thus, in the present case studies, the bulk of the currents producing the magnetic variations are located in the magnetosphere (magnetopause and ring current), implying that most of the curl of the equivalent current system is concentrated near the geomagnetic poles, which are pretty far from our area. In consequence, when HAD is used as a validation point (so that its data are not considered in the SECS inversion), the method allocates the curl at HAD latitudes, thereby distorting the results for this station. It is worth to note, however, that the performance improves considerably when the boundary of the grid area is extended northward, so that the poles are allowed to be located at higher latitudes.

We also confirm the results of *McLay and Beggan* [2010] that the use of internal sources for SECS does not improve the performance of the interpolation for the horizontal components of the magnetic field with respect to the use of external only (i.e., ionospheric) sources.

Figure 3 shows the north component of the magnetic field extrapolated using the above described techniques at Mesón do Vento, one of the substations of the Spanish power network, in occasion of St. Patrick's storm (17–18 March 2015). Note that this is not a validation point, since this northwesternmost part of the country is devoid of geomagnetic observatories. We also note that for the different field continuation techniques, AQU observatory has been replaced by VAL (−10.3°E, 51.9°N) in this case. We confirm that the different methods are in relative agreement, except perhaps for the NN method, which gives somewhat lower values. For the east component the agreement is even better. In conclusion, any of the proposed interpolation methods is suitable enough for the study of GICs in the Spanish power grid.

2.2. Obtaining Empirical Impedance Tensors

In a previous study [*Torta et al.*, 2014], GICs were modeled in the neutral of a transformer of the Vandellòs substation using EBR geomagnetic values (NN method) since it is only 36 km away (Figure 1). The performance of the model was analyzed in terms of the structure of the Earth conductivity, and its predictions were compared with real measurements in the occasion of a geomagnetic storm in 24–25 October 2011. That was one of the first relevant events of solar cycle 24, on which the planetary *K* index was 7 and the *Dst* reached values of −137 nT [*Blanch et al.*, 2013]. Using a homogeneous and isotropic ground conductivity of 10^{-3} S/m, a reasonable correlation coefficient of 0.36 was obtained, but the 1-D conductivity models obtained from the available magnetotelluric (MT) studies in this area [*Pous et al.*, 1995] did not improve substantially the ones obtained by the homogenous Earth approach, suggesting the need of incorporating the effect of lateral heterogeneities. This is especially important because the lateral conductivity contrast is large

at land-sea interfaces, making the 1-D assumption probably invalid in the Mediterranean coastal area [e.g., *Falgàs et al.*, 2009; *Rosell et al.*, 2011].

The use of MT data can address this problem directly. In the MT method, the impedance tensor, Z, can be obtained in the frequency domain by linearly relating the horizontal electric and magnetic fields measured at the site:

$$\vec{E}_h(T) = \frac{1}{\mu} Z(T) \, \vec{B}_h(T), \tag{2}$$

where T is the period (note that we use the period instead of the frequency) and μ is the magnetic permeability of the Earth which, in most situations, can be taken as that of the free space, μ_0. The elements of the MT impedance, $Z_{ij}, i, j{=}1, 2$, are traditionally represented by the apparent resistivity, ρ_a, and the phase, φ, given by

$$\rho_{a,ij}(T) = \frac{T}{2\pi\mu} \left| Z_{ij} \right|^2, \qquad\qquad \varphi_{ij}(T) = \tan^{-1}\left(\frac{\text{Im}\,(Z_{ij})}{\text{Re}\,(Z_{ij})} \right). \tag{3}$$

GICs at a particular transformer are related with the horizontal electric field by means of a dot product for long periods (low frequencies), given in the time domain (4a) and in the frequency domain (4b) as

$$\text{gic}(t) = \vec{a}\,' \cdot \vec{e}_h(t), \tag{4a}$$

$$\text{GIC}(T) = \vec{a}\,' \cdot \vec{E}_h(T), \tag{4b}$$

where the prime indicates the transpose of a vector or a matrix, and the elements of $\vec{a}$ are scale values accounting for the properties of a particular transformer of the power network. These transformer properties only depend on the geometry and resistances of the network when considering that the horizontal electric field is uniform, meaning that $\vec{a}$ can be taken as a network constant for each transformer [*Lehtinen and Pirjola*, 1985; *Pirjola and Lehtinen*, 1985]. The vector $\vec{a}$ gives the direction of electric field producing the maximum values of GIC, while its modulus provides the proportionality factor to obtain the maximum values of GIC for a specified electric field amplitude [*Torta et al.*, 2014; *Boteler and Pirjola*, 2017].

The MT impedance near the substation can be considered as the representative response of the regional geoelectrical structure for long periods. If we substitute (2) into (4b), we obtain

$$\text{GIC}(T) = \frac{1}{\mu} \vec{a}\,' \, Z(T) \, \vec{B}_h(T), \tag{5}$$

which summarizes the relation between the three factors listed in section 1: the knowledge of the geomagnetic field variations ($\vec{B}_h$), the knowledge of the Earth's geoelectrical structure (Z), and the knowledge of the power grid elements ($\vec{a}$).

To obtain Z, a MT sounding in the Vandellòs substation area was acquired. The MT site was located 6 km farther inland to find a suitable quieter location to reduce the effect of the anthropogenic electromagnetic noise. The acquisition was performed with two types of MT instruments: an ADU-06 Metronix system with induction coils for shorter periods (10^{-3}–3 s) and a Spider Worldsensing datalogger with Bartington fluxgate magnetometers for the longer periods ($2 \cdot 10^1 - 2 \cdot 10^4$ s). The electric field components were measured in NS and EW directions using nonpolarizable copper sulfate electrodes. The shorter period data ($<$10 s) were recorded during 2 h by the Metronix instrument and the longer period data ($>$10 s) during 12 days (19 February 2015 to 2 March 2015) by the Spider-Bartington system.

The processing of the time series to obtain Z was performed with robust methods. The shorter period data were processed with Mapros software [*Friedrichs*, 2007]. The longer period data were processed with the birrp code [*Chave and Thomson*, 2004], applying both the Estimation of Local transfer-functions by

Apparent Resistivity
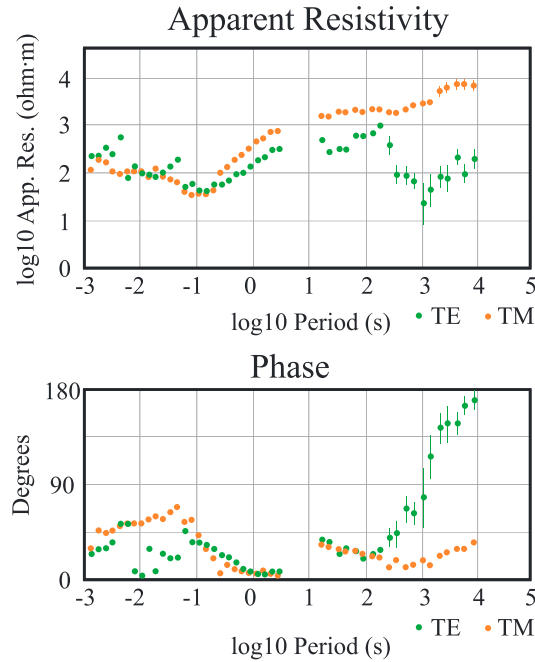
Phase

Figure 4. Measured (top) apparent resistivity and (bottom) phase versus period according to the TE (green) and TM (orange) modes at the vicinity of Vandellòs substation. Error bars are uncertainties at 68.2% of confidence.

Combining Interstation Transfer-functions (ELICIT) [*Campanyà et al.*, 2014] and remote reference [*Gamble et al.*, 1979] methods with geomagnetic data from EBR and CLF magnetic observatories (Figure 1).

The analysis of the long period data was performed by means of the Goom-Bayley decomposition using the strike code [*McNeice and Jones*, 2001], showing that these data were compatible with a 2-D regional structure with a strike of N37.8°. This result coincides with the direction of the coast in this area (N38°). The MT impedance tensor was accordingly rotated N38° to obtain the so-called Transverse Magnetic (TM) and Transverse Electric (TE) modes, which are oriented parallel and perpendicular to the strike direction (the coastline), respectively. In Figure 4, the curves of apparent resistivity and phase versus period of these two modes are plotted, neither of which shows evidences of galvanic effects.

Four different approaches were tested to reproduce the electric fields used to model the GIC at the Vandellòs station: Homogeneous background, 1-D and 2-D approaches, and the full tensor Z.

1. The homogeneous model was the same as in *Torta et al.* [2014], assuming for this approach the impedance of a background resistivity model of 1000 ohm m.
2. For the 1-D approach we performed the determinant approach, which provides a representative value of the Z tensor for each period [*Berdichevsky and Dmitriev*, 1976]:

$$Z_{1D}(T) = \sqrt{Z_{11}(T)Z_{22}(T) - Z_{12}(T)Z_{21}(T)}.$$ (6)

3. For the 2-D approach we have obtained the results shown in Figure 4. They present the typical behavior consisting in a lateral conductor (the sea) where the TE curve is below the TM curve in a given range of periods [*Ledo*, 2005]. Since the GIC computation is based on a dot product, which is rotationally invariant, we can rewrite (5) in the rotated direction θ (= 38°) as

$$\mathrm{GIC}(T) = \frac{1}{\mu}\,\vec{a}'R'_\theta\,Z_\theta(T)R_\theta\,\vec{B}_h(T) = \frac{1}{\mu}\,\vec{a}'_\theta\,Z_\theta(T)\,\vec{B}_{h\theta}(T),$$ (7a)

or in components

$$\mathrm{GIC}(T) = \frac{1}{\mu}(a\ b)\begin{pmatrix} \cos\theta & -\sin\theta \\ \sin\theta & \cos\theta \end{pmatrix}\begin{pmatrix} 0 & Z_{TE} \\ -Z_{TM} & 0 \end{pmatrix}\begin{pmatrix} \cos\theta & \sin\theta \\ -\sin\theta & \cos\theta \end{pmatrix}\begin{pmatrix} B_x(T) \\ B_y(T) \end{pmatrix}$$ (7b)

where a and b are the north and east components of $\vec{a}$; Z_{TE} and Z_{TM} are the TE and TM surface impedances, respectively, obtained as explained above, and B_x and B_y are the north and east geomagnetic field components, respectively.
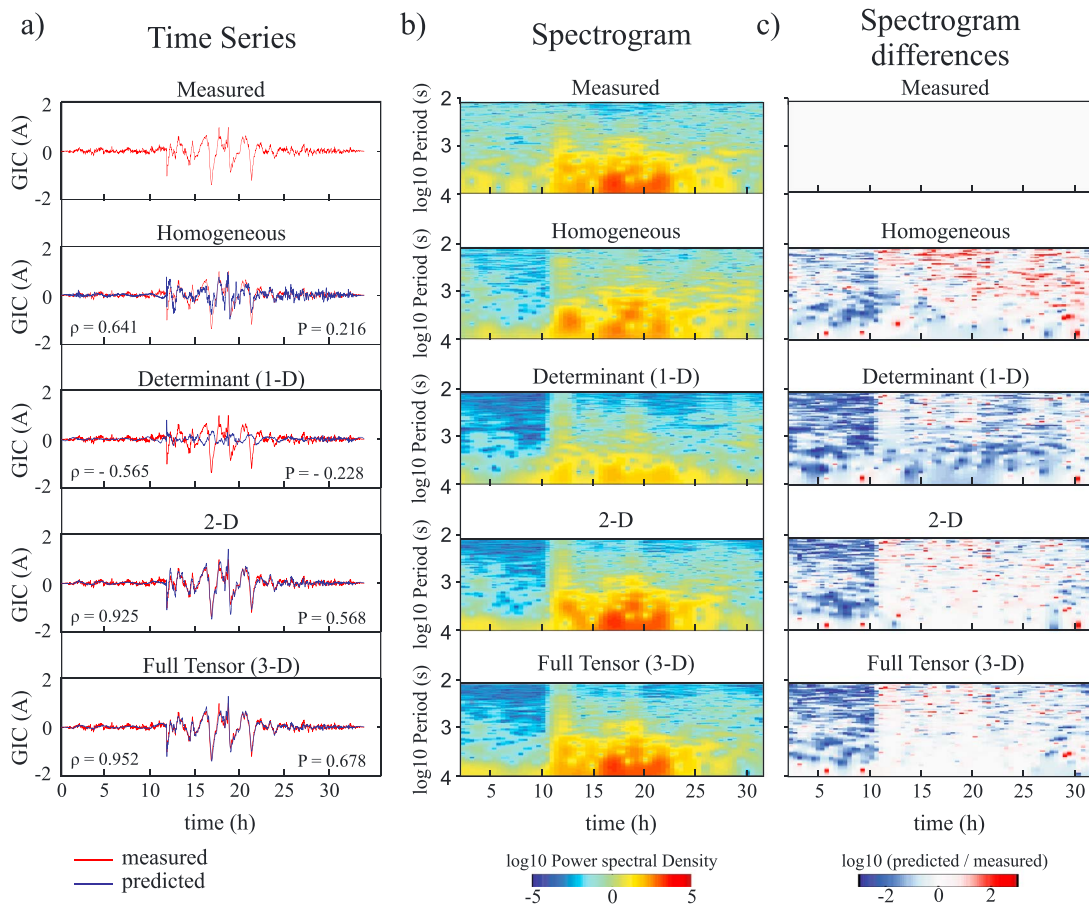
Figure 5. Comparison of (a) time series, (b) spectrograms, and (c) spectrogram differences at the TRP1 transformer in Vandellòs for the October 24–25 2011 event corresponding to (first row) measurements and different modeling approaches: (second row) homogeneous, (third row) determinant (1-D), (fourth row) 2-D, and (fifth row) full tensor (3-D). A band-pass filter was applied to the original time series to take into account only periods in the range 200–10,000 s.

4. Finally, we computed the GIC using the full tensor Z, without the need to apply any rotation.

We first evaluated the performance of all the proposed approaches (homogeneous, 1-D, 2-D, and full tensor) focusing only on periods in the range 200–10,000 s. These boundaries were constrained by the sampling rate (1 min) at measuring the GIC at the Vandellòs substation and by the quality of the tensor Z (Figure 4). To take into account only this period range, a band-pass filter was applied to the original time series.

Results are shown in Figure 5, comparing the fit with the measured GIC in the time domain (using again the NN as the source field interpolation method), with the correlation coefficient and performance parameter, and in the frequency domain by comparing the associated spectrograms (variation of the energy at each analyzed period along time). High accuracy was observed in the time and frequency domains when performing either the 2-D approach or the full tensor Z, obtaining a P greater than 0.5 and a correlation coefficient above 0.9. In the frequency domain, the ratio between modeled and measured GIC is close to 1 during the storm for most of the periods. Note that before the storm, during the first 10 h, the predicted GIC is underestimated (blue in Figure 5c), probably due to the presence of signal in the power transmission network not related to the geomagnetic activity. On the other hand, the GICs predicted by means of the homogeneous and 1-D approaches are less accurate (in both the time and frequency domains), and as observed by *Torta et al.* [2014], the homogeneous approach using 1000 ohm m provides better results than the 1-D approach because the 1-D approach underestimates the signal for most of the analyzed periods in this case. These results show that the regional geoelectrical response is strongly affected by the Mediterranean Sea, which implies that the homogeneous and 1-D approaches are not appropriate to reproduce the complexity (2-D environment) of the surface electric fields, while the 2-D approach and the full tensor are. Note that no major improvement is observed when using the full tensor instead of the 2-D approach.
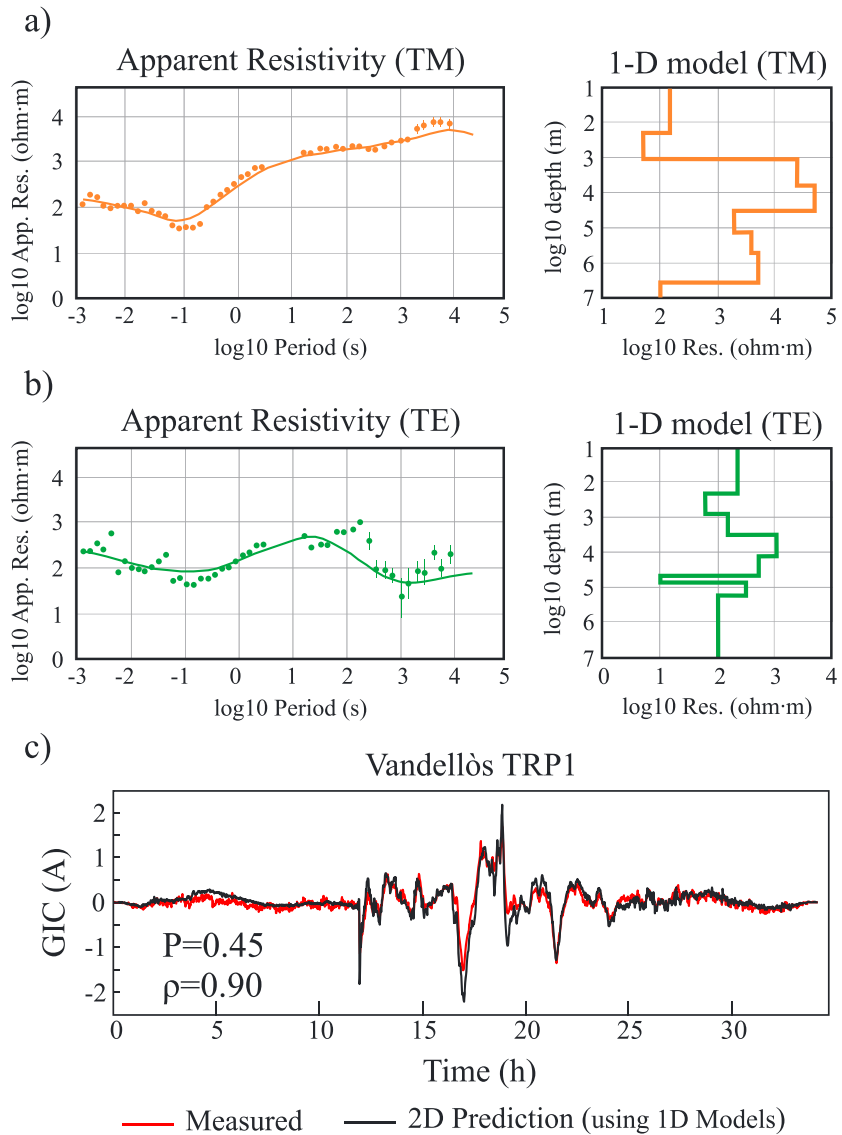
Figure 6. One-dimensional conductivity models (right) that fit the (a) TM and (b) TE apparent resistivity curves at the vicinity of Vandellòs substation. Their fitting is at left. (c) Measured (red) and calculated (black) GIC at the TRP1 transformer in Vandellòs for the October 24–25 2011 event using the 2-D approach consisting of the TM and TE modes.

In this case, the homogeneous approach, not based on the measured MT impedance tensor, provided better results than the 1-D approach using the determinant of the MT impedance tensor. However, both approaches overestimate and underestimate the amplitudes for most of the periods (Figures 5b and 5c), being unable to reproduce the influence of the more complex geoelectrical structures around the area of interest. Note that with the 1-D approach we are averaging structures located below the site with structures away from the site such as the Mediterranean Sea, without differentiating their contribution to the different components of the MT impedance tensor. Probably, if the area was 1-D, the 1-D approach would have provided a more accurate result improving the homogeneous model.

Finally, we removed the band-pass filter and looked at all periods, including periods longer than 10,000 s for which quality data of the Z tensor worsen. Using the 2-D approach as the simplest case that better fits the data in the Vandellòs substation, we inverted the two 1-D layered models that only fit the apparent resistivity for each mode (TE and TM) using the algorithm developed by *Constable et al.* [1987]. Although these models are physically meaningless, they reproduce the measured impedances, and, as they propagate to infinite

Table 1. Quantification of the Goodness of Our Model Predictions During Different Storms[a]

Day	ρ	P
9–13 September 2011	0.81	0.14
24–25 October 2011	0.90	0.45
22 January 2012	0.84	0.21
26–27 February 2012	0.87	0.29
8–9 March 2012	0.89	0.40
16–17 June 2012	0.89	0.35

[a]The table shows the quantification of the goodness of our model predictions with respect to the GIC measurements at the TRP1 transformer in the Vandellòs substation for different events according to the linear correlation coefficient, ρ, and the performance parameter P.

depth, they allow us to extrapolate, as a first approach, the values of the MT impedance tensor for periods longer than 10,000 s. The 1-D models and their fittings are presented in Figures 6a and 6b. The GIC predicted by this "all-period" 2-D approach is compared with the measured GIC in Figure 6c (now without any filter applied). We obtained a ρ of 0.90 and a P of 0.45, which support the proposed approach for extrapolating the signal at longer periods. Similar results (ρ between 0.81 and 0.90 and P between 0.14 and 0.45) were obtained for the six storms recorded during September 2011 to June 2012, the only period when actual GIC measurements are available at that transformer (see Table 1). The same a and b constants that account for the resistances and topology of the grid were used, although it might have happened that during some of those storms some transmission lines were switched off. The differences of the ρ and P values observed between Figures 5 and 6c for the 2-D approach are mainly caused by periods longer than 10,000 s.

Thus, although the available GIC measurements at Vandellòs substation only lasted for 10 months, with our network model and the surface impedance measurements, we have the response of the transformers to the geomagnetic disturbances reasonably well characterized in that substation, having demonstrated the importance of reproducing the dimensionality of the geoelectrical structures at the point of interest when predicting GICs.

2.3. Sensitivity to Network Changes

A perfect match between GIC model predictions and observations is never possible because of the assumed simplifications. A useful guide for the relative importance of the system parameters when estimating GIC impacts on a power network is given in *Zheng et al.* [2014]. The power network is much complex, including systems of less than 400 kV voltages, which are galvanically connected to the higher voltage grid through autotransformers. For simplification, we completely ignored the autotransformers' low-voltage circuits, assuming the winding resistance as the sum of the common and the series resistances. Fortunately at Vandellòs substation, where we performed the comparison analysis, there are neither autotransformers nor full-wound transformers. However, this substation connects with others that have such autotransformers, and this may have some influence on the circulation of GICs. In addition, the information relating to the resistances of all the transformers and lines was incomplete, so that we had to assume typical values for most of the earthing resistances, for several winding resistances, and for a few unknown line resistances.

In order to assess the extent to which the above mentioned simplifications can affect the model behavior, we performed a sensitivity analysis to network resistance changes in the way suggested by *Kelly et al.* [2016]. A first test was made by evaluating the model performance at the same Vandellòs substation in the occasion of the geomagnetic storm in October 2011 when the total earthing resistances of each transformer

Figure 7. Quantification of the goodness of our model predictions with respect to the GIC measurements at the TRP1 transformer in the Vandellòs substation for the event of 24–25 October 2011, when scaling the earthing resistances of the grid by the factor C, according to the performance parameter P.
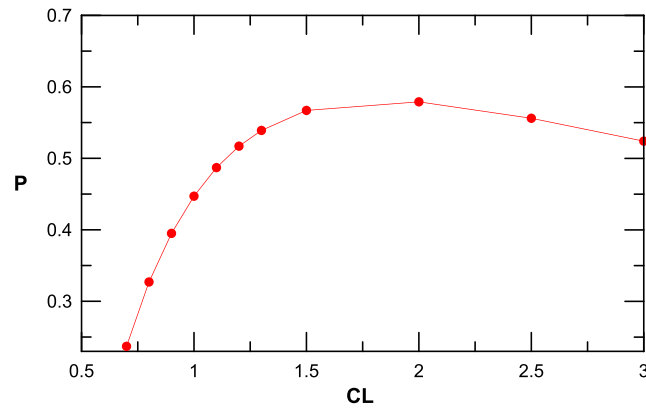
Figure 8. Quantification of the goodness of our model predictions with respect to the GIC measurements at the TRP1 transformer in the Vandellòs substation for the event of 24–25 October 2011, when scaling the line resistances of the grid by the factor *CL*, according to the performance parameter *P*.

in the grid (including their winding resistances and the actual substation grounding resistance) are multiplied by a common factor, *C*, taken to be between 0.5 and 5. Results are given in Figure 7. Notice that the model fit reduces drastically when the earthing resistances decrease. *P* is, however, less sensitive to resistance increases, though a smooth improvement is detected as they grow, reaching a maximum increase of 14 percentage points when *C* = 2.5. The correlation coefficient, on the contrary, is insensitive to changes in the earthing resistances across the whole network, which means that as expected, they do not have any effect on the induced current waveforms but only on the current amplitudes. For a given inducing magnetic field and a given network electric circuit topology, induced signal waveforms are only a function of the geoelectrical structure. It is another matter when there are changes in the grid topology. Switching on or off the key transmission lines or transformers is essential to decrease or boost significant currents through the remaining elements. This certainly affects the current amplitudes, but depending on the orientation of the added or removed line, it can also affect its waveforms since, in general, it will differently affect the north and east network constants. In the same way, if the earthing resistance changes were not made uniformly, both network constants had not been scaled equally.

A similar analysis was carried out by changing the line resistances of the whole grid through another scale factor, which we named *CL*, while keeping the former, *C*, equal to 1. *CL* was allowed to vary between 0.7 and 1.3 at 0.1 steps, and between 1.5 and 3.0 at 0.5 steps (Figure 8). Again, reducing the resistances from their nominal values leads to a decrease of the model performance, while increasing them improves the parameter *P*. The maximum improvement, of roughly 13 percentage points, is reached when *CL* = 2. Again, being the changes made uniformly across the whole grid, the experiment did not affect the linear correlation between the model and the observations.

Finally, we were tempted to examine the effect of setting *C* = 2.5 and *CL* = 2, but this did not produce better performances than changing either the earthing or the line resistances independently. That improvement of 14 percentage points seems to be the upper limit that we can reach if we leave the system to just change according to the circuit resistances.

3. Discussion and Conclusions

Previous to this work, we had examined the hazard from space weather to the Spanish high-voltage grid by providing comprehensive estimates of the expected GIC values through the grid. The power companies can use our results in their risk assessment, which are certainly both scientifically and practically useful. However, the predictions can be affected by intrinsic limitations of modeling, and in this new study we have assessed some of these limitations.

We first analyzed the impact of different computation methods of the true variation of the geomagnetic field at the network substation under consideration. We have confirmed that SECS is not necessarily the most adequate method for magnetic field interpolation purposes at midlatitudes during disturbed periods, so that simpler techniques such as the "nearest neighbor" or a low-degree polynomial fit to the magnetic scalar potential are suitable enough. In other words, the method employed to interpolate/extrapolate the magnetic field variations is a minor cause of uncertainty in the calculation of GICs at the Spanish power network, a result that probably applies to middle latitudes in general.

Second, to improve the accuracy of the GIC estimations, we demonstrated how magnetotelluric measurements allow obtaining the empirical MT impedance that properly represents the response of the regional geological structure, including lateral heterogeneities, like land-ocean interfaces. Results based on approaches that cannot reproduce the dimensionality of the geoelectrical structures are significantly worse than the approaches that are capable of doing it. The test performed also showed that the use of 1-D models in the approach of the elements of the 2-D impedance tensor can improve the prediction of GICs. The reason is that they behave smoother than data, especially when the quality of data worsens for some range of periods, e.g., at longer periods. In comparison with the previously used uniform or 1-D layered structures, the model performance in our test site improved by a factor of 2.4 in terms of the correlation coefficient and a factor greater than 8 in terms of the more suitable performance parameter. This remarkable improvement has been achieved even though we have imposed uniformity, throughout the whole grid, on the derived geoelectric field in the vicinity of the substation of concern. The simplification probably worked because the substations that connect with it have similar geoelectric conditions (analogous terrains, similar proximity to the coastline, and same strike), and even if the conditions are different at farther stations, they have much less influence on the currents flowing in the neutral of the inspected transformer. Thus, in this example, we observed that the predicted GICs rely more on the suitable geoelectrical structure (dimensionality) than on the assumption of uniformity of the horizontal electric field, but this behavior cannot be widespread. While it would be desirable to benefit from a dense survey of MT measurements such as the EarthScope in the United States [*Bedrosian and Love*, 2015], local surveys as the one described in this paper can represent a practical solution in grid nodes identified as hazardous to the threat posed by GICs.

Finally, despite the difficulties of obtaining accurate values of the network parameters (e.g., the true resistance values of the lines or the transformer windings or their connections to the ground), the sensitivity analysis has shown that the approximate values for network parameters can be still satisfactory for the GIC computation.

Though there is still room for improvement, we have shed some more light to progress in the three aspects that we had identified as fundamental to get an appropriate GIC vulnerability analysis for our country: (i) we have developed and tested a tool to get the geomagnetic field variations at each node of the grid; (ii) we have quantified and evaluated the contribution of several aspects of the MT impedance tensor when computing GIC, and (iii) we have evaluated the importance of the relative resistances of the power grid, though more important than this is the exact knowledge of the active elements during each geomagnetic storm. Lessons learnt from this and our previous GIC assessments can be used to determine both mitigation strategies and relevant locations for installing monitoring equipment. At those critical sites, MT measurements and the use of a reasonable approach in agreement with the dimensionality of the geoelectrical structures at the sites of interest are essential to improve the matching between the model predictions and actual observations.

References

Amm, O. (1997), Ionospheric elementary current systems in spherical coordinates and their applications, *J. Geomagn. Geoelectr.*, 49, 947–955.

Amm, O., and A. Viljanen (1999), Ionospheric disturbance magnetic field continuation from the ground to the ionosphere using spherical elementary current systems, *Earth Planets Space*, 51, 431–440.

Baker, D. N. (2016), Becoming a space weather-ready nation, *Space Weather*, 1–2, doi:10.17226/13060.

Barbosa, C., L. Alves, R. Caraballo, G. A. Hartmann, A. R. R. Papa, and R. J. Pirjola (2015), Analysis of geomagnetically induced currents at a low-latitude region over the solar cycles 23 and 24: Comparison between measurements and calculations, *J. Space Weather Space Clim.*, 5, 9, doi:10.1051/swsc/2015036.

Bedrosian, P. A., and J. J. Love (2015), Mapping geoelectric fields during magnetic storms: Synthetic analysis of empirical United States impedances, *Geophys. Res. Lett.*, 42, 10,160–10,170, doi:10.1002/2015GL066636.

Berdichevsky, M. N., and V. I. Dmitriev (1976), Distortion of magnetic and electric fields by near surface lateral inhomogeneities, *Acta Geod. Geophys. Montan. Acad. Sci. Hung.*, 11, 447–483.

Blake, S. P., P. T. Gallagher, J. McCauley, A. G. Jones, C. Hogg, J. Campanyà, C. Beggan, A. W. P. Thomson, G. S. Kelly, and D. Bell (2016), Geomagnetically induced currents in the Irish power network during geomagnetic storms, *Space Weather*, 14, 1136–1154, doi:10.1002/2016SW001534.

Blanch, E., S. Marsal, A. Segarra, J. M. Torta, D. Altadill, and J. J. Curto (2013), Space weather effects on Earth's environment associated to the 24–25 October 2011 geomagnetic storm, *Space Weather*, 11, 153–168, doi:10.1002/swe.20035.

Boteler, D. H., and R. J. Pirjola (2017), Modeling geomagnetically induced currents, *Space Weather*, 15, 258–276, doi:10.1002/2016SW001499.

Campanyà, J., J. Ledo, P. Queralt, A. Marcuello, M. Liesa, and J. A. Muñoz (2011), Lithospheric characterization of the Central Pyrenees based on new magnetotelluric data, *Terra Nova*, 23, 213–219.

Campanyà, J., J. Ledo, P. Queralt, A. Marcuello, M. Liesa, and J. A. Muñoz (2012), New geoelectrical characterization of a continental collision zone in the west-central Pyrenees: Constraints from long period and broadband magnetotellurics, *Earth Planet. Sci. Lett.*, *333–334*, 112–121.

Campanyà, J., J. Ledo, P. Queralt, A. Marcuello, and A. G. Jones (2014), A new methodology to estimate magnetotelluric (MT) tensor relationships: Estimation of Local transfer-functlons by Combining Interstation Transfer-functions (ELICIT), *Geophys. J. Int.*, *198*, 484–494.

Carter, B. A., E. Yizengaw, R. Pradipta, A. J. Halford, R. Norman, and K. Zhang (2015), Interplanetary shocks and the resulting geomagnetically induced currents at the equator, *Geophys. Res. Lett.*, *42*, 6554–6559, doi:10.1002/2015GL065060.

Chave, A. D., and D. J. Thomson (2004), Bounded influence magnetotelluric response function estimation, *Geophys. J. Int.*, *157*(3), 988–1006.

Constable, S. C., R. L. Parker, and C. G. Constable (1987), Occam's inversion—A practical algorithm for generating smooth models from electromagnetic sounding data, *Geophysics*, *52*(03), 289–300.

Delaunay, B. (1934), Sur la sphere vide. A la mémoire de Georges Voronoi, *Bull. Acad. Sci. USSR*, *6*, 793–800.

Demiray, T., G. Beccuti, and G. Andersson (2013), Risk assessment of the impact of geomagnetic disturbances on the transmission grid in Switzerland, *IEEE Power Energy Soc. Gen. Meet.*, doi:10.1109/PESMG.2013.6672600.

Düzgit, Z., N. Baydemir, and S. R. C. Malin (1997), Rectangular polynomial analysis of the regional geomagnetic field, *Geophy. J. Int.*, *128*, 737–743.

Fiori, R. A. D., D. H. Boteler, and D. M. Gillies (2014), Assessment of GIC risk due to geomagnetic sudden commencements and identification of the current systems responsible, *Space Weather*, *12*, 76–91, doi:10.1002/2013SW000967.

Falgàs, E., J. Ledo, A. Marcuello, and P. Queralt (2009), Monitoring freshwater-seawater interface dynamics with audiomagnetotelluric data, *Near Surf. Geophys.*, *7*(5–6), 391–399.

Friedrichs, B. (2007), MAPROS, Magnetotelluric processing software (Metronix), User Manual.

Gamble, T. D., J. Clarke, and W. M. Goubau (1979), Magnetotellurics with a remote magnetic reference, *Geophysics*, *44*(1), 53–68.

Gilbert, J. L. (2014), Simplified techniques for treating the ocean-land interface for geomagnetically induced electric fields, in *Proceedings of the IEEE International Symposium on Electromagnetic Compatibility*, pp. 566–569, IEEE, Raleigh, N. C.

Jonas, S., and E. McCarron (2015), Recent U.S. policy developments addressing the effects of geomagnetically induced currents, *Space Weather*, *13*, 730–733, doi:10.1002/2015SW001310.

Kappenman, J. G. (2003), Storm sudden commencement events and the associated geomagnetically induced current risks to ground-based systems at low-latitude and midlatitude locations, *Space Weather*, *1*(3), 1016, doi:10.1029/2003SW000009.

Kelly, G. S., A. Viljanen, C. D. Beggan, A. W. P. Thomson, and A. Ruffenach (2016), Understanding GIC in the UK and French high voltage transmission systems during severe magnetic storms, *Space Weather*, *15*, 99–114, doi:10.1002/2016SW001469.

Knipp, D. J. (2015), Synthesis of geomagnetically induced currents: Commentary and research, *Space Weather*, *13*, 727–729, doi:10.1002/2015SW001317.

Lehtinen, M., and R. J. Pirjola (1985), Currents produced in earthed conductor networks by geomagnetically-induced electric fields, *Ann. Geophys.*, *3*, 479–484.

Liu, C., Y. Li, and R. Pirjola (2014), Observations and modeling of GIC in the Chinese large-scale high-voltage power networks, *J. Space Weather Space Clim.*, *4*, 3–9, doi:10.1051/swsc/2013057.

Ledo, J. (2005), 2-D versus 3-D magnetotelluric data interpretation, *Surv. Geophys.*, *26*(5), 511–543.

Ledo, J., A. G. Jones, A. Siniscalchi, J. Campanyà, D. Kiyan, G. Romano, and TopoMed MT Team (2011), Electrical signature of modern and ancient tectonic processes in the crust of the Atlas mountains of Morocco, *Phys. Earth Planet. Inter.*, *185*(3), 82–88.

Love, J. J. (2012), Credible occurrence probabilities for extreme geophysical events: Earthquakes, volcanic eruptions, magnetic storms, *Geophys. Res. Lett.*, *39*, L10301, doi:10.1029/2012GL051431.

Marsal, S., J. M. Torta, A. Segarra, and T. Araki (2017), Use of spherical elementary currents to map the polar current systems associated with the geomagnetic sudden commencements on 2013 and 2015 St. Patrick's Day storms, *J. Geophys. Res. Space Physics*, *122*, 194–211, doi:10.1002/2016JA023166.

McLay, S. A., and C. D. Beggan (2010), Interpolation of externally-caused magnetic fields over large sparse arrays using spherical elementary current systems, *Ann. Geophys.*, *28*, 1795–1805, doi:10.5194/angeo-28-1795-2010.

McNeice, G. W., and A. G. Jones (2001), Multisite, multifrequency tensor decomposition of magnetotelluric data, *Geophysics*, *66*(1), 158–173.

Ngwira, C. M., A. A. Pulkkinen, E. Bernabeu, J. Eichner, A. Viljanen, and G. Crowley (2015), Characteristics of extreme geoelectric fields and their possible causes: Localized peak enhancements, *Geophys. Res. Lett.*, *42*, 6916–6921, doi:10.1002/2015GL065061.

Nikitina, L., L. Trichtchenko, and D. H. Boteler (2016), Assessment of extreme values in geomagnetic and geoelectric field variations for Canada, *Space Weather*, *14*, 481–494, doi:10.1002/2016SW001386.

Piña-Varas, P., J. Ledo, P. Queralt, A. Marcuello, R. Hidalgo, and M. Messeiller (2014), 3-D magnetotelluric exploration of Tenerife geothermal system (Canary Islands, Spain), *Surv. Geophys.*, *35*(4), 1045–1064.

Piña-Varas, P., J. Ledo, P. Queralt, A. Marcuello, F. Bellmunt, X. Ogaya, N. Pérez, and J. A. Rodriguez-Losada (2015), Vertical collapse origin of Las Cañadas caldera (Tenerife, Canary Islands) revealed by 3-D magnetotelluric inversion, *Geophys. Res. Lett.*, *42*, 1710–1716, doi:10.1002/2015GL063042.

Pirjola, R. J. (2013), Practical model applicable to investigating the coast effect on the geoelectric field in connection with studies of geomagnetically induced currents, *Adv. Appl. Phys.*, *1*(1), 9–28.

Pirjola, R. J., and M. Lehtinen (1985), Currents produced in the Finnish 400 kV power transmission grid and tin the Finnish natural gas pipeline by geomagnetically-induced electric fields, *Ann. Geophys.*, *3*, 485–492.

Pous, J., J. Ledo, A. Marcuello, and M. Daignières (1995), Electrical resistivity model of the crust and upper mantle from a magnetotelluric survey through the central Pyrenees, *Geophy. J. Int.*, *121*(3), 750–762.

Pulkkinen, A. (2016), Introduction to NASA Living With a Star (LWS) Institute GIC Working Group Special Collection, *Space Weather*, doi:10.1002/2016SW001537.

Pulkkinen, A., E. Bernabeu, J. Eichner, C. Beggan, and A. W. P. Thomson (2012), Generation of 100-year geomagnetically induced current scenarios, *Space Weather*, *10*, 1–37, doi:10.1029/2011SW000750.

Riley, P., and J. J. Love (2017), Extreme geomagnetic storms: Probabilistic forecasts and their uncertainties, *Space Weather*, *15*, 53–64, doi:10.1002/2016SW001470.

Rosell, O., A. Martí, A. Marcuello, J. Ledo, P. Queralt, E. Roca, and J. Campanyà (2011), Deep electrical resistivity structure of the northern Gibraltar Arc (western Mediterranean): Evidence of lithospheric slab break-off, *Terra Nova*, *23*(3), 179–186.

Thomson, A. W. P., E. B. Dawson, and S. J. Reay (2011), Quantifying extreme behaviour in geomagnetic activity, *Space Weather*, *9*, S10001, doi:10.1029/2011SW000696.

Torta, J. M., L. Serrano, J. R. Regué, A. M. Sánchez, and E. Roldán (2012), Geomagnetically induced currents in a power grid of northeastern Spain, *Space Weather*, *10*, S06002, doi:10.1029/2012SW000793.

Torta, J. M., S. Marsal, and M. Quintana (2014), Assessing the hazard from geomagnetically induced currents to the entire high-voltage power network in Spain, *Earth Planets Space*, *66*(1), 1–17, doi:10.1186/1880-5981-66-87.

Wintoft, P., A. Viljanen, M. Wik, and A. Viljanen (2016), Extreme value analysis of the time derivative of the horizontal magnetic field and computed electric field, *Ann. Geophys.*, *34*(4), 485–491, doi:10.5194/angeo-34-485-2016.

Zhang, J. J., C. Wang, T. R. Sun, C. M. Liu, and K. R. Wang (2015), GIC due to storm sudden commencement in low-latitude high-voltage power network in China: Observation and simulation, *Space Weather*, *13*, 643–655, doi:10.1002/2015SW001263.

Zheng, K., D. H. Boteler, R. Pirjola, L. G. Liu, R. Becker, and S. Guillon (2014), Influence of system characteristics on the amplitudes of geomagnetically induced currents, *IEEE Trans. Power Deliv.*, *29*(2), 1–9.